Atmospheric carbon dioxide linked with Mesozoic and early Cenozoic climate change

BENJAMIN J. FLETCHER[1], STUART J. BRENTNALL[1], CLIVE W. ANDERSON[2], ROBERT A. BERNER[3] AND DAVID J. BEERLING[1]*

[1]Department of Animal and Plant Sciences, University of Sheffield, Sheffield S10 2TN, UK
[2]Department of Probability and Statistics, University of Sheffield, Sheffield S10 2TN, UK
[3]Department of Geology and Geophysics, Yale University, New Haven, Connecticut 06520, USA
*e-mail: d.j.beerling@sheffield.ac.uk

Published online: 9 December 2007; doi:10.1038/ngeo.2007.29

The relationship between atmospheric carbon dioxide (CO_2) and climate in the Quaternary period has been extensively investigated, but the role of CO_2 in temperature changes during the rest of Earth's history is less clear[1]. The range of geological evidence for cool periods during the high CO_2 Mesozoic 'greenhouse world'[2,3] of high atmospheric CO_2 concentrations, indicated by models[4] and fossil soils[5], has been particularly difficult to interpret. Here, we present high-resolution records of Mesozoic and early Cenozoic atmospheric CO_2 concentrations from a combination of carbon-isotope analyses of non-vascular plant (bryophyte) fossils and theoretical modelling[6,7]. These records indicate that atmospheric CO_2 rose from ~420 p.p.m.v. in the Triassic period (about 200 million years ago) to a peak of ~1,130 p.p.m.v. in the Middle Cretaceous (about 100 million years ago). Atmospheric CO_2 levels then declined to ~680 p.p.m.v. by 60 million years ago. Time-series comparisons show that these variations coincide with large Mesozoic climate shifts[8–10], in contrast to earlier suggestions of climate–CO_2 decoupling during this interval[1]. These reconstructed atmospheric CO_2 concentrations drop below the simulated threshold for the initiation of glaciations[11] on several occasions and therefore help explain the occurrence of cold intervals in a 'greenhouse world'[3].

The fundamental role of CO_2 as a driver of past warm climates in the Mesozoic and early Cenozoic periods remains obscured for a number of reasons. Different proxies (fossil leaf stomatal indices and palaeosols) yield widely disparate CO_2 estimates for this critical phase in Earth's history[3]; in general, palaeosols[5] suggest CO_2 levels thousands of p.p.m.v. higher than fossil leaves[12]. Furthermore, it is unclear whether mismatches between oxygen-isotope-based ($\delta^{18}O$) palaeoclimate records and ancient CO_2 estimates[1], either from proxies or numerical carbon-cycle models[2–4], genuinely reflect decoupling between CO_2 and climate or are an artefact associated with the difficulties of accurately reconstructing these critical features of Earth's history[13]. However, evidence for brief (typically < 1 Myr) cool pulses punctuating generally warm Jurassic and Cretaceous climates is challenging the prevailing high CO_2 Mesozoic 'greenhouse world' paradigm[3] indicated by palaeosols[5] and geochemical carbon-cycle models[4].

Here, we report a series of CO_2 estimates for the ancient atmosphere reaching back over 200 Myr, by using a new method based on the strong dependency of carbon-isotope fractionation ($\Delta^{13}C$) in terrestrial bryophytes on atmospheric CO_2 during photosynthetic carbon uptake[6,7]. The approach is the terrestrial analogue of the marine phytoplankton CO_2 proxy[14], successfully used to reconstruct glacial–interglacial CO_2 changes from Pleistocene peat cores[15]. In functional terms, $\Delta^{13}C$ approaches the maximum fractionation value (~30‰) expressed by the primary carboxylating enzyme ribulose-1,5-carboxylase/oxygenase (RuBisCo), as the CO_2 concentration at the site of fixation (C_i) approaches the external CO_2 concentration (C_a) (refs 6,7). Because C_i is set by the combined influence of net photosynthetic CO_2 uptake (A) and resistance to the inward diffusion of CO_2 (r), $\Delta^{13}C$ is proportional to C_i/C_a, where $C_a - C_i = A \times r$. In bryophytes, r is not subject to stomatal control, as in the leaves of vascular plants, and $\Delta^{13}C$ varies with C_a and the photosynthetic demand for CO_2 by RuBisCo (refs 6,7).

We estimated ancient atmospheric CO_2 concentrations on the basis of 93 $\delta^{13}C$ measurements on 61 liverwort gametophyte compression fossils (Fig. 1a–d). The fossils spanned 150 Myr and were sampled from 12 localities on 5 continents (Table 1). Conversion of $\delta^{13}C$ measurements to palaeoatmospheric CO_2 concentrations is achieved after calculating $\Delta^{13}C$ to account for variations in the $\delta^{13}C$ of atmospheric CO_2 (Table 1), and inverting a well-validated mechanistic mathematical model (BRYOCARB) describing the CO_2 dependency of $\Delta^{13}C$ in bryophytes[7]. All calculated fossil $\Delta^{13}C$ values lie within the range sensitive to variations in CO_2, except those for the Palaeocene (Ypresian) specimens (Fig. 1e, inset). BRYOCARB models $\Delta^{13}C$ as a function of C_i/C_a, which is determined by the balance between photosynthetic CO_2 draw-down and diffusional CO_2 supply to the tissue from the atmosphere. Photosynthesis is represented with established biochemical theory for CO_2 assimilation and explicitly accounts for the interactive effects of irradiance, O_2 and temperature[7] (see the Supplementary Information for derivation of values). The supply of CO_2 from the atmosphere to the site of photosynthesis is modelled by analogy with Ohm's law[7]. BRYOCARB$_P$ calibrates $\Delta^{13}C$ change in liverworts with pores, where

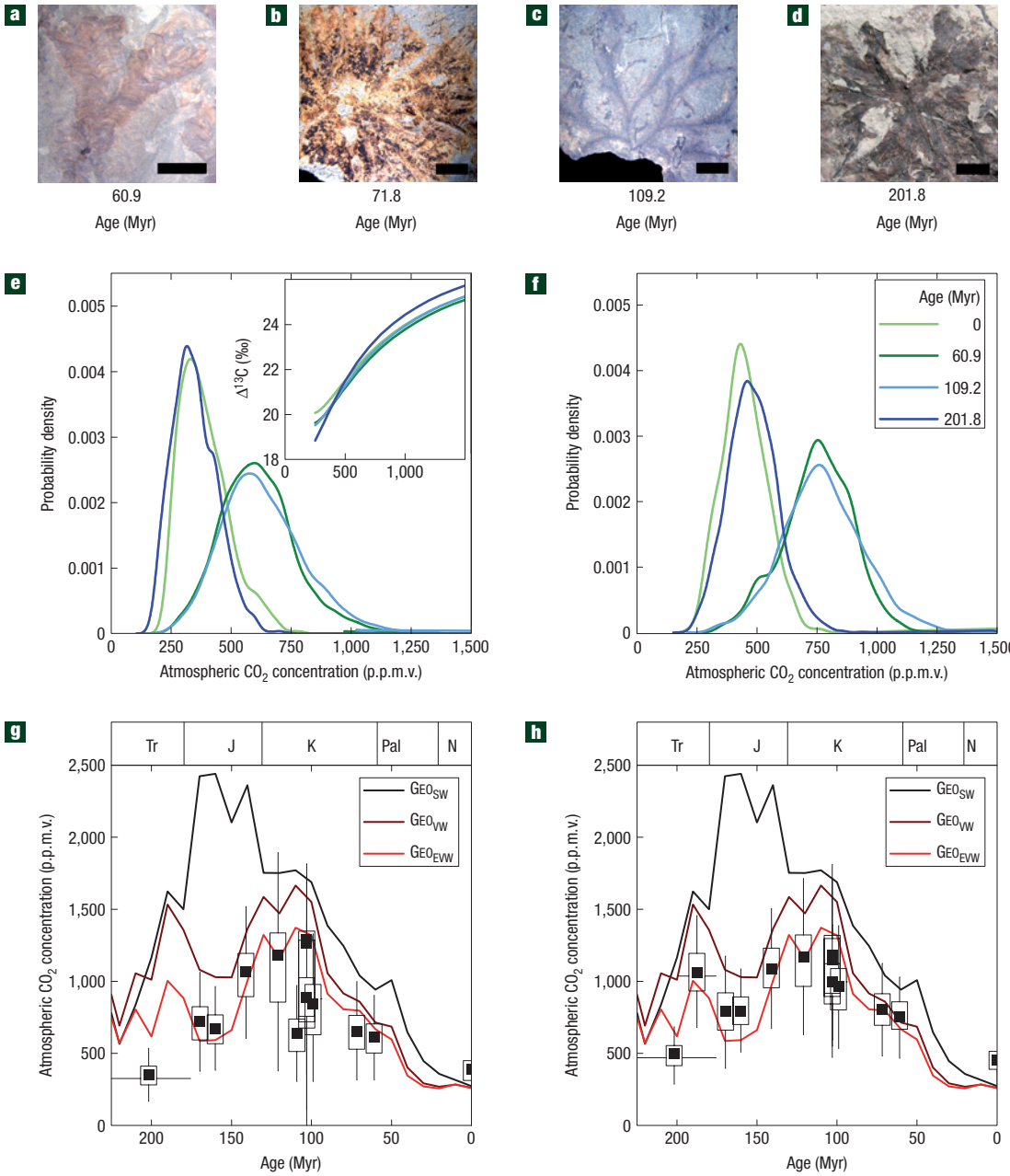

Figure 1 Atmospheric CO_2 concentrations from fossil liverworts. a–d, Example liverwort compression fossils. All scale bars are 5 mm. **e**,**f**, Example PDFs of CO_2 concentrations estimated from fossil liverwort $\Delta^{13}C$ calibrated with $BRYOCARB_P$ (**e**) and $BRYOCARB_{NP}$ (**f**). Inset: Modelled response of $\Delta^{13}C$ to CO_2 for fossils **a**,**c** and **d**. **g**,**h**, Reconstructed CO_2 histories using fossil liverwort $\Delta^{13}C$ and $BRYOCARB_P$ (**g**) and $BRYOCARB_{NP}$ (**h**). The CO_2 histories predicted by a geochemical model with formulations for standard[18] (GEO_{SW}), moderate[20,21] (GEO_{VW}) and enhanced[19] (GEO_{EVW}) volcanic weathering are also shown (with the latter two assuming very low rates of basalt seawater reaction). Squares indicate means, error bars and boxes, the 10–90% and 25–75% uncertainty ranges respectively. Tr: Triassic, J: Jurassic, K: Cretaceous, Pal: Palaeocene, N: Neogene.

r is regulated by varying pore density and morphology. However, some groups of liverworts lack pores and are unable to regulate *r* in this way. Because these are not always distinguishable as fossils, we used a second version of the model, $BRYOCARB_{NP}$, to calibrate $\Delta^{13}C$ changes in liverworts without pores, with a prescribed resistance and a lower maximum rate of RuBisCo-limited carboxylation (V_{cmax}; see the Supplementary Information)[6]. Uncertainties for each CO_2 estimate are characterized by deriving probability density functions (PDFs) using large (25,000) ensemble Monte Carlo simulations to integrate uncertainties in inferred and measured input variables for both versions of BRYOCARB (see the Methods section).

Our new atmospheric CO_2 reconstruction, spanning approximately one-third of the Phanerozoic eon (the past 540 Myr), exhibits coherent trends throughout the Mesozoic and early Cenozoic (Fig. 1g–h). These trends primarily reflect CO_2-driven systematic shifts of up to 5‰ in fossil bryophyte $\Delta^{13}C$; other environmental inputs play a secondary role in determining the

Table 1 Details of fossil liverworts and their mean ($\pm 1\sigma$) stable-carbon-isotope composition ($\delta^{13}C$) and fractionation ($\Delta^{13}C$). Specimen numbers, species lists and provenances are given in Supplementary Information.

Period (stage)*	Age (Myr ago)	Location	Palaeolat.	Species†	$\delta^{13}C_p$‡ (‰) (*n*)	$\delta^{13}C_a$ (‰)§	$\Delta^{13}C$ (‰)¶
Modern	0	UK	52° N	4 liverwort spp. (Tp)	−29.50±1.36 (18)	−10.04±0.21	19.95±1.36
				4 liverwort spp. (Tnp)	−28.64±0.98 (10)	−10.14±0.20	19.15±1.00
Pal (Ypresian)	48.6–55.8	Amurskya, E. Russia	54° N	*Marchantites* sp. (T)	−30.35±0.60 (3)	−4.87±0.22	27.14±0.66
Pal (Selandian–Thanetian)	55.8–61.0	Montana, USA	52° N	Unspecified liverwort (T)	−25.01±0.76 (5)	−4.13±0.32	22.28±0.83
K (M Maastrichtian)	71.6–71.9	Wyoming, USA	56° N	Unspecified liverwort (T)	−26.25±1.00 (1)	−4.89±0.01	22.80±1.00
K (L Albian–Cenomanian)	93.5–104.6	S. Is., New Zealand	73° S	Unspecified liverwort (L)	−28.41±1.00 (1)	−5.08±0.45	24.87±1.10
K (L Albian)	99.6–106.4	Alexander Is., Antarctica	72° S	Unspecified liverwort (T)	−28.13±0.88 (9)	−4.73±0.46	24.94±1.00
				Thallites bicostatus (T)	−28.56±1.17 (3)	−4.73±0.46	25.39±1.26
				Marchantites spp. (T)	−28.54±1.34 (4)	−4.73±0.46	25.38±1.42
K (E Albian)	106.4–112.0	SW. Alberta, Canada	57° N	*Marchantiolites blairmorensis* (Tp)	−25.26±0.97 (15)	−4.14±0.45	22.53±1.08
K (Barremian–Aptian)	112.0–130.0	Amurskya, E. Russia	58° N	*Striatothallus adniancus* (T)	−27.36±0.60 (5)	−4.34±1.10	24.53±1.26
K (L Berriasian–E Valanginian)	139.0-143.0	E. Sussex, UK	38° N	*Hepaticites zeilleri* (T)	−27.72±1.00 (1)	−5.82±0.06	23.38±1.01
J (Callovian–Oxfordian)	155.7–164.7	Amurskya, E. Russia	58° N	*Cheirorhiza brittae* (L)	−26.20±1.00 (5p)	−5.22±0.41	22.41±1.08
J (M Bajocian)	167.7–171.6	Yorkshire, UK	39° N	*Hepaticites arcuates* (T)	−25.68±1.32 (3)	−5.54±0.41	21.54±1.38
J (Hettangian–Toarcian)	175.6–199.6	Greenland	49° N	*Ricciopsis* sp. (Tnp)	−27.43±1.00 (1)	−5.35±0.45	23.57±1.10
Tr–J (Carnian–Toarcian)	175.6–228.0	Transantarctic Mtns, Antarctica	66° S	Unspecified liverwort (T)	−24.44±1.00 (1)	−5.26±0.66	20.52±1.20

*Ages from ref. 27. Tr: Triassic, J: Jurassic, K: Cretaceous, Pal: Palaeocene.

†Nomenclature follows ref. 28; leafy (L) or thallose (T) species with pores (p) or no pores (np) indicated where known.

‡Fossil $\delta^{13}C_p$ measurements corrected by -2.35 ± 0.57‰ to account for diagenesis as determined by the shift in extant liverwort $\delta^{13}C$ after chemical macerations to remove non-structural materials ($n=6$ species)[6]; (*n*) = number of fossils analysed separately or pooled (*p*) in the case of samples with small amounts of carbon. Reported σ values were obtained from the summed variances for $\delta^{13}C_p$ and the diagenesis adjustment factor; measurements on single specimens were assigned a mean variance for all fossil samples.

§Calculated from the mean of stratigraphically widespread low-Mg calcitic skeletons[29] and a composite open ocean Atlantic Deep Sea Drilling Project bulk marine carbonate record[30]. For fossil samples, $\delta^{13}C_a$ is calculated with an offset of -7.0 ± 0.13‰ (ref. 4) with the error given by temperature effects on calcium bicarbonate dissolution[6]. Reported σ values obtained from the variation within the age uncertainty of the fossils, except for Jurassic samples for which the Deep Sea Drilling Project record may not reflect a global signal. These samples have been assigned a σ value from the mean variance for the Cretaceous record. $\delta^{13}C_a$ is calculated for modern samples with an offset of -1.89 ± 0.16‰ to account for anthropogenic influences relative to ocean-based flask measurements[6].

¶Calculated as $\Delta^{13}C\ (‰) = (\delta^{13}C_a - \delta^{13}C_p)/(1+\delta^{13}C_p/1{,}000)$, where $\mathrm{Var}(\Delta^{13}C) = g(\delta^{13}C_p, \delta^{13}C_a) \cong (\partial g/\partial\delta^{13}C_a)^2\mathrm{Var}(\delta^{13}C_a) + (\partial g/\partial\delta^{13}C_p)^2\mathrm{Var}(\delta^{13}C_p)$.

pattern (see the Supplementary Information). CO_2 estimates derived from fossil bryophyte $\Delta^{13}C$ calibrated using either BRYOCARB$_P$ or BRYOCARB$_{NP}$ both rise from comparatively low concentrations in the Triassic and Early Jurassic to a peak of ~1,130 p.p.m.v. in the Middle Cretaceous, and then decline towards 680 p.p.m.v. in the early Cenozoic (Fig. 1g–h). Calibrated $\Delta^{13}C$ changes using BRYOCARB$_{NP}$ lead to CO_2 estimates approximately 60 p.p.m.v. higher than those using BRYOCARB$_P$, as the increased resistance to inward CO_2 diffusion meant that a higher C_a is required to reproduce the C_i/C_a inferred from fossil $\Delta^{13}C$. The only exception to the coherent trend is a singular high CO_2 estimate during the Ypresian (48.6–55.8 Myr ago, 2,300–4,740 p.p.m.v.), which may reflect the reduced sensitivity of the bryophyte proxy at high CO_2 and should therefore be regarded as less certain than the others. Although we recognize that it coincides with peak Cenozoic warmth, until better understood by investigation of further fossil materials, we have omitted this from our subsequent time-series analyses.

We used the bryophyte CO_2 records to evaluate the role of this greenhouse gas in the evolution of Mesozoic and early Cenozoic warm climates by calculating CO_2-forced temperatures for comparison with independent palaeoclimate records. Cross-correlation coefficients were computed between the resulting changes in mean global surface temperature (ΔT) and a pH-adjusted tropical surface ocean temperature series based on the $\delta^{18}O$ of marine calcium carbonate fossils[1,16], after accounting for uncertainties in ΔT due to imperfect knowledge of vital effects[1], post-depositional alteration[9] and the $\delta^{18}O$ of ocean water[17] (see the Methods section). Other evidence supports the major pattern revealed by the pH-adjusted $\delta^{18}O$ record showing cooler Middle Jurassic (160–167 Myr ago)[8] and warmer Cretaceous climates[9,10], suggesting that it is a useful metric for evaluating greenhouse forcing by calculated CO_2 trends. Agreement between calculated and observed changes in ΔT was quantified using a hierarchical curve reconstruction technique accommodating the irregular spacing of $CO_2/\Delta T$ determinations and uncertainties in their estimation and dating (see the Methods section). The same approach was also used to evaluate CO_2 as a driver of climate change using an extensive compilation of CO_2 estimates derived from studies of fossil leaves and palaeosols[3].

Results indicate that the bryophyte and stomatal CO_2 histories reproduce the average Mesozoic climate, yielding average global temperatures within 0.7 °C of that estimated from the pH-adjusted $\delta^{18}O$ climate record (Fig. 2a,b). In contrast, calculated temperatures with palaeosol CO_2 histories were 2.0–2.5 °C higher than the marine record (Fig. 2b). Cross-correlations revealed that only ΔT patterns calculated from the CO_2 histories of fossil bryophytes were positively correlated with ΔT from the marine $\delta^{18}O$ record (median coefficients = 0.2–0.5; Fig. 2c,d). Neither the stomatal nor the palaeosol proxies produced positive correlations with independent records of climate (Fig. 2d). The capacity of the bryophyte proxy to describe both overall temperatures and the magnitude of climate change may be evidence for CO_2 forcing of major climatic shifts, but this suggestion requires assessment of the reliability of each of the three proxies used to reconstruct ancient atmospheric CO_2 concentrations.

We therefore benchmarked proxy performance against the predictions of numerical carbon-cycle models to identify those most consistent with known variations in the long-term sources and sinks for CO_2. Comparisons were made with a series of three atmospheric CO_2 histories simulated using a coupled carbon–oxygen–sulphur cycle geochemical model[18] that incorporated different representations of basalt weathering to describe the range of field observations[19,20]. Treatment of all other CO_2 source and sink terms remained unchanged in each of the following three simulations: (1) standard weathering[18] (GEO$_{SW}$), (2) moderate weathering linked to variations in the production and exposure of volcanic rocks[21] assuming unusually low values for

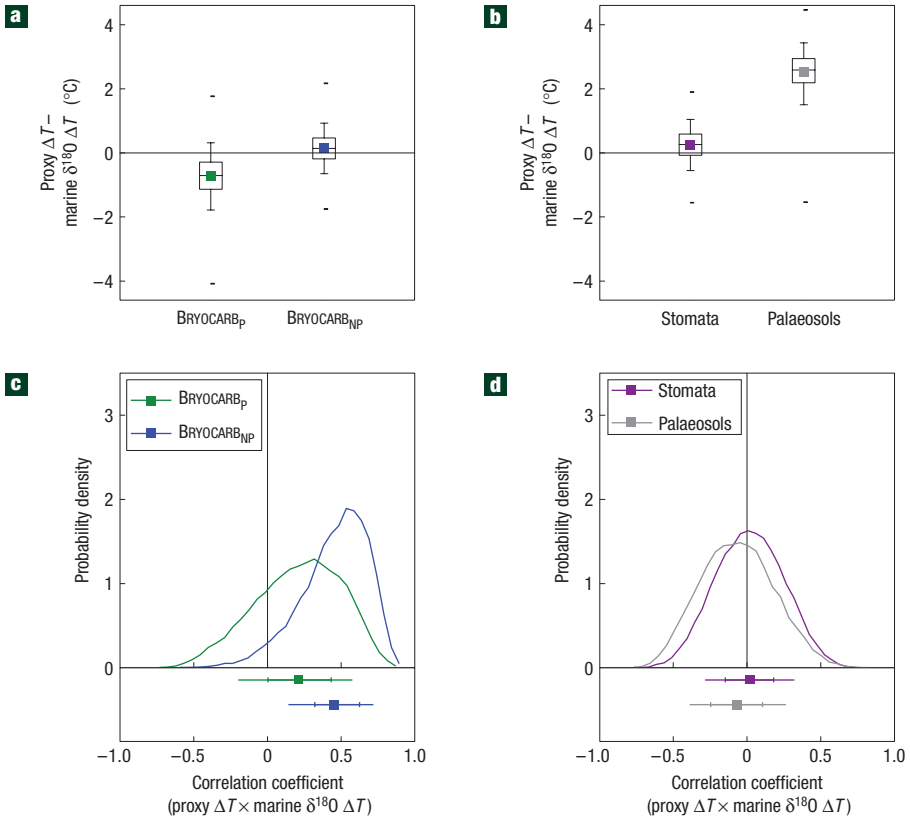

Figure 2 Evaluation of CO_2 forcing with reconstructed changes in temperature (ΔT). a,**b**, Absolute mean difference in ΔT between proxies and $\delta^{18}O$ records over the Mesozoic. Points represent the mean, the box the 25–75% range, and the horizontal lines across the box plot the median. Error bars represent the 10–90% range and short horizontal lines the extreme values. **c**,**d**, PDFs of the correlation between normalized ΔT calculated from the proxy CO_2 records, and $\delta^{18}O$ records. Squares indicate means, error bars and boxes, the 10–90% and 25–75% uncertainty ranges respectively.

basalt–seawater (BSW) reaction rate (GEO_{VW}), and (3) as (2) but with enhanced weathering of basalts[19] and very low BSW rates or with moderate weathering and reasonable BSW rates (GEO_{EVW}) (see the Methods section). Proxy performance was defined with summary statistics for absolute differences in proxy–model CO_2 values integrated over the Mesozoic and early Cenozoic, and correlation coefficients between proxy–model CO_2 time series (see the Methods section).

These comparisons indicate that fossil bryophytes provide a more coherent record of fluctuations in Earth's atmospheric CO_2 content over the Mesozoic and early Cenozoic than either of the other two existing proxies covering the same interval. Fossil bryophytes and the stomatal proxy estimated CO_2 concentrations lower than all three model simulations, but this underestimation was progressively reduced from ~−750 p.p.m.v. to only ~−90 p.p.m.v. with increasing emphasis on the weathering of volcanic silicates (Fig. 3a–c). In contrast, the palaeosol proxy considerably overestimated CO_2 values, increasing from ~+590 p.p.m.v. to ~+1,370 p.p.m.v. across the same series of simulations (Fig. 3d). The closest agreement between two out of three proxies with GEO_{EVW} strengthens the case for variations in the production and exposure of basalts as playing a prominent role in regulating CO_2 levels on a multimillion-year timescale[19,21]. However, cross-correlation analyses indicate that only the bryophyte proxy was both a good fit and exhibited a positive correlation in the trends in CO_2 simulated with GEO_{VW} and GEO_{EVW} (Fig. 3e–h). This suggests that the bryophyte proxy has accuracy and captures some patterns of the CO_2 histories simulated by these two versions of the geochemical model. Neither of the other two proxies fulfilled both criteria simultaneously. The stomatal CO_2 proxy record correlated best with GEO_{SW} CO_2 predictions, but this simulation gave the largest CO_2 difference (Fig. 3c,g). The palaeosol proxy CO_2 record was not strongly correlated with any of the three model simulations, and had CO_2 concentrations different from model results (Fig. 3d,h).

We conclude that CO_2 forcing played an important role in Mesozoic and early Cenozoic climate change, and that earlier claims for a decoupling in the CO_2–climate relationship during this critical phase in Earth's history[1] are premature. Changes in the CO_2 greenhouse effect, driven by geochemical controls on the long-term carbon cycle[4,21], thus contribute an explanation for Jurassic and Cretaceous climates without the need to invoke the influence of cosmic rays on cloud cover and planetary albedo[22]. Furthermore, our reconstructed CO_2 concentrations (500–1,300 p.p.m.v., Fig. 1) coincide with the threshold for the initiation of glaciations determined by global climate modelling calibrated for mid-Cenozoic conditions[11] (560–1,120 p.p.m.v.). Although the exact range is likely to be dependent on the particular climate model, CO_2 histories derived from palaeosols[5] and earlier geochemical carbon-cycle models[4] exceed this threshold by several thousand p.p.m.v. Our new CO_2 reconstructions therefore offer a resolution for the high CO_2 'greenhouse world' paradox by better explaining the apparent susceptibility of the Earth system to experience brief discrete cool events during the Mesozoic[3].

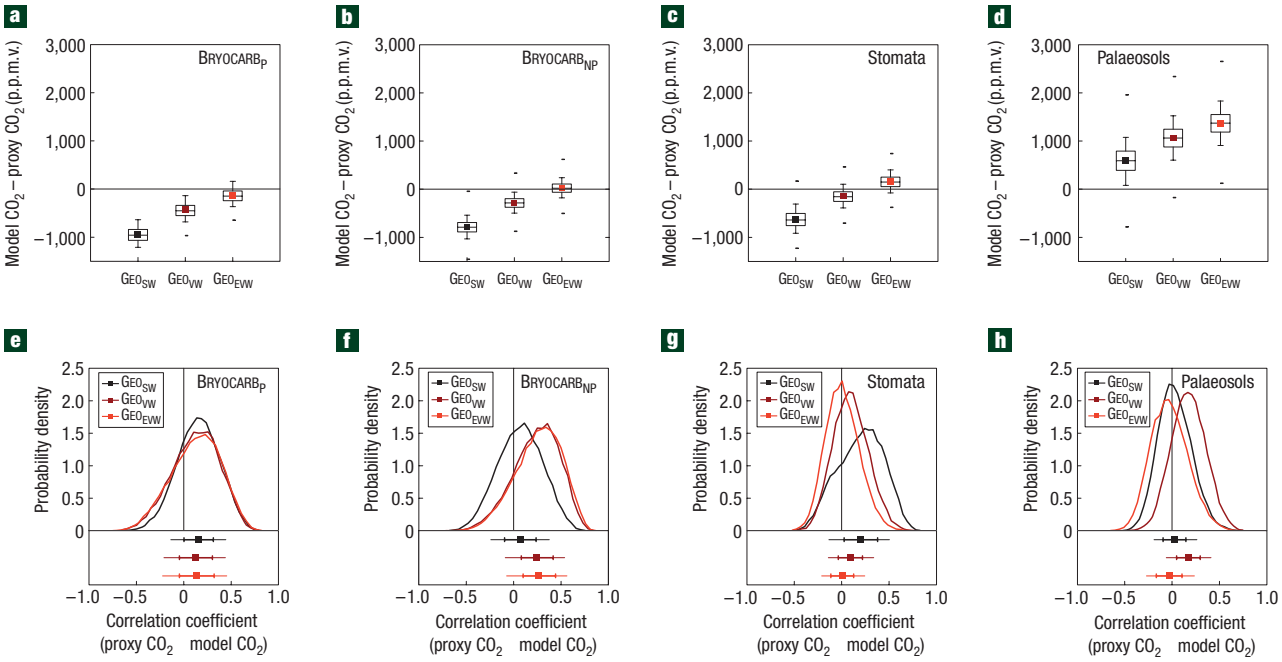

Figure 3 Comparison of proxy and geochemical model CO_2 estimates. a–d, Difference in average CO_2 concentration between models and proxies. **e–h**, PDFs of the correlation between normalized model and proxy CO_2 records. Box plot and horizontal errors as for Fig. 2.

METHODS

UNCERTAINTY ANALYSIS OF BRYOPHYTE CO_2 ESTIMATES

PDFs characterizing uncertainty in CO_2 determinations were estimated from 25,000 Monte Carlo simulations of the derivation based on alternative values of physiological (V_{cmax}, respiration rate, diffusion resistance and response of resistance to CO_2) and environmental (temperature, O_2 and irradiance) parameters (see the Supplementary Information) and $\Delta^{13}C$ including errors in measuring/estimating $\delta^{13}C_p$ and $\delta^{13}C_a$ (Table 1). Values were sampled from either normal or truncated normal distributions with dispersion parameters obtained from the literature, measurement errors (Fig. 1e,f) and, in the case of diffusion resistance and its response to CO_2, nonlinear regression fitting of data from modern specimens. The possibilities of uncertainty in dependence between physiological parameters, irradiance and $\Delta^{13}C$ were allowed for. Variations in water content of field populations of liverworts exert minimal effects on $\Delta^{13}C$ and are excluded from the analyses[6,7]. The resulting uncertainty PDF for CO_2 is interpreted in the Bayesian sense as a representation of rational belief.

STATISTICAL COMPARISONS OF TIME SERIES

To compare proxy CO_2 estimates with model predictions, and to compare calculated and observed ΔT, we used a hierarchical curve reconstruction technique that accommodates the irregular spacing of CO_2 determinations and allows for uncertainty in both their estimation and dates. At the first stage, synthetic sets of CO_2–age/ΔT–age values were generated from uncertainty distributions derived here or on the basis of reports in the literature. For CO_2 estimates based on the bryophyte, stomata and palaeosol proxies, and models, we used log-normal distributions representing uncertainties derived from this letter, from reported errors for replicate leaves and palaeosols[3], and an error envelope determined from earlier multiparameter sensitivity analyses[4], respectively. Uncertainties in ΔT due to imperfect knowledge of the $\delta^{18}O$ of ocean water, diagenesis and vital effects, and ages were represented with normal distributions[1]. Age uncertainties for proxies were represented by uniform distributions based on reported dating error ranges[3].

At the second stage, for each resulting synthetic data set a continuous interpolant for CO_2 or ΔT consistent with conditional uncertainty (given the discrete data points) about the rate and magnitude of changes between data points was generated from a gaussian stochastic process with a powered exponential covariance kernel. Parameters were adjusted to represent likely fluctuations in the relationship of magnitudes around 250 p.p.m.v. per million years for CO_2, consistent with ice-core data[23] or equivalent values for ΔT using the same radiative forcing function[4]. The simulated histories resulting from the combined stages represent samples from the uncertainty distributions of the respective continuous functional relationships[24].

A measure of the agreement between two functional relationships over a time interval T is given by the integrated correlation $r = \int_T x(t)y(t)dt$, where $x(t)$ and $y(t)$ are the functions representing the relationships standardized to zero mean and the unit integrated square over T; generally $|r| \leq 1$, and $r = 1$ indicates perfect agreement. The PDF of r was estimated by kernel density estimation[25] from the ensembles of curves, and measures the agreement between histories, taking account of their respective uncertainties.

PALAEOCLIMATE ESTIMATES

We calculated CO_2 forcing using a simple CO_2 greenhouse forcing function that accounts for solar evolution and the logarithmic relationship to CO_2 concentration, with a moderate equilibrium climate sensitivity[4] ($2 \times CO_2$ $\Delta T = 2.3\,^{\circ}C$). Tropical surface ocean $\delta^{18}O$ temperatures[1] were converted by dividing by 0.87 to approximate global surface values and facilitate comparisons with the CO_2 forcing function[26]. An important caveat with this exercise is that the marine $\delta^{18}O$ record includes a pH adjustment based on CO_2 from a geochemical model that revises ΔT estimates upwards[16]. Lower CO_2 concentrations, from either bryophyte records or the GEO_{EVW} simulation, would revise temperatures down by $\sim$0.5 °C over the Mesozoic.

GEOCHEMICAL MODEL CO_2 CALCULATIONS

The volcanic-corrected GEOCARBSULF model[18,21] was used to calculate atmospheric CO_2 concentrations by varying values of W_v/W_{nv} and NV. W_v and W_{nv} are the rates of weathering per unit mass respectively of volcanic and non-volcanic Ca and Mg silicates. Values used here were $W_v/W_{nv} = 1$ for GEO_{SW} (GEOCARBSULF with no volcanic effect[18]), $W_v/W_{nv} = 2$ for GEO_{VW} (moderate volcanic effect[20]) and $W_v/W_{nv} = 10$ for GEO_{EVW} (enhanced volcanic effect[19]). Both volcanic effects assume very low BSW reaction rates. More realistic BSW values give results for $W_v/W_{nv} = 2$ similar to those for low BSW and $W_v/W_{nv} = 10$. NV is a parameter that relates the deviation of the global mean $^{87}Sr/^{86}Sr$ from the present value (0.717) for non-volcanic Ca and Mg silicate weathering. Its value is uncertain and can only be crudely estimated.

We use NV = 0 for GEO_{VW} and NV = 0.01 for GEO_{EVW}. The use of NV = 0.01 and $W_v/W_{nv} = 10$ for GEO_{EVW} applies only to very low BSW reaction rates and leads to a maximum effect on CO_2 of changes in volcanic exposure.

Received 23 May 2007; accepted 11 October 2007; published 9 December 2007.

References

1. Veizer, J., Godderis, Y. & François, L. M. Evidence for decoupling of atmospheric CO_2 and global climate during the Phanerozoic eon. *Nature* **408**, 698–701 (2000).
2. Royer, D. L., Berner, R. A., Montanez, I., Tabor, N. J. & Beerling, D. J. CO_2 as a primary driver of Phanerozoic climate change. *GSA Today* **14**, 4–10 (2004).
3. Royer, D. L. CO_2-forced climate thresholds during the Phanerozoic. *Geochim. Cosmochim. Acta* **70**, 5665–5675 (2006).
4. Berner, R. A. *The Phanerozoic Carbon Cycle* (Oxford Univ. Press, Oxford, 2004).
5. Ekart, D. D., Cerling, T. E., Montañez, I. P. & Tabor, N. J. A 400 million year carbon isotope record of pedogenic carbonate: implications for paleoatmospheric carbon dioxide. *Am. J. Sci.* **299**, 805–827 (1999).
6. Fletcher, B. J., Beerling, D. J., Brentnall, S. J. & Royer, D. L. Fossil bryophytes as recorders of ancient CO_2 levels: Experimental evidence and a Cretaceous case study. *Global Biogeochem. Cycles* **19**, (2005) (doi:10.1029/2005GB002495).
7. Fletcher, B. J., Brentnall, S. J., Quick, W. P. & Beerling, D. J. BRYOCARB: A process-based model of thallose liverwort carbon isotope fractionation in response to CO_2, O_2, light and temperature. *Geochim. Cosmochim. Acta* **70**, 5676–5691 (2006).
8. Dromart, G. *et al.* Ice age at the Middle-Late Jurassic transition? *Earth Planet. Sci. Lett.* **213**, 205–220 (2003).
9. Wilson, P. A., Norris, R. D. & Cooper, M. J. Testing the Cretaceous greenhouse hypothesis using glassy foraminiferal calcite from the core of the Turonian tropics on Demerara Rise. *Geology* **30**, 607–610 (2002).
10. Shouten, S. *et al.* Extremely high sea-surface temperatures at low latitudes during the middle Cretaceous as revealed by archeal membrane lipids. *Geology* **31**, 1069–1072 (2003).
11. DeConto, R. M. & Pollard, D. Rapid Cenozoic glaciation of Antarctica induced by declining atmospheric CO_2. *Nature* **421**, 245–249 (2003).
12. Retallack, G. J. A 300-million-year record of atmospheric carbon dioxide from fossil plant cuticles. *Nature* **411**, 287–290 (2001).
13. Kump, L. R. Reducing uncertainty about carbon dioxide as a climate driver. *Nature* **419**, 188–190 (2002).
14. Freeman, K. H. & Hayes, J. M. Fractionation of carbon isotopes by phytoplankton and estimates of ancient CO_2 levels. *Global Biogeochem. Cycles* **6**, 185–198 (1992).
15. White, J. W. C., Ciais, P., Figge, R. A., Kenny, R. & Markgraf, V. A high-resolution record of atmospheric CO_2 content from carbon isotopes in peat. *Nature* **367**, 153–156 (1994).
16. Ridgwell, A. A mid Mesozoic revolution in the regulation of ocean chemistry. *Mar. Geol.* **217**, 339–357 (2005).
17. Roche, D. M., Donnadieu, Y., Pucéat, E. & Paillard, D. Effects of changes in $\delta^{18}O$ content of the surface ocean on estimated sea surface temperatures in past warm climates. *Paleoceanography* **21**, (2006) (doi:10.1029/2005PA001220).
18. Berner, R. A. GEOCARBSULF: A combined model for Phanerozoic atmospheric O_2 and CO_2. *Geochim. Cosmochim. Acta* **70**, 5653–5664 (2006).
19. Dessert, C., Dupre, B., Gaillardet, J., Francios, L. M. & Allegre, C. J. Basalt weathering laws and the impact of basalt weathering on the global carbon. *Chem. Geol.* **202**, 257–273 (2003).
20. Taylor, A. S. *Chemical Weathering Rates and Sr Isotopes*. Thesis, Yale Univ., New Haven (2000).
21. Berner, R. A. Inclusion of the weathering of volcanic rocks in the GEOCARBSULF model. *Am. J. Sci.* **306**, 295–302 (2006).
22. Wallmann, K. Impact of atmospheric CO_2 and galactic cosmic radiation on Phanerozoic climate change and the marine $\delta^{18}O$ record. *Geochem. Geophys. Geosyst.* **5**, (2004) (doi:10.1029/2003GC000683).
23. Siegenthaler, U. *et al.* Stable carbon cycle-climate relationship during the late Pleistocene. *Science* **310**, 1313–1317 (2005).
24. Ramsay, J. O. & Silverman, B. W. *Functional Data Analysis* 2nd edn (Springer, New York, 2005).
25. Silverman, B. W. *Density Estimation for Statistics and Data Analysis* (Chapman & Hall, London, 1986).
26. Beerling, D. J. & Woodward, F. I. *Vegetation and the Terrestrial Carbon Cycle. Modelling the First 400 Million Years* (Cambridge Univ. Press, Cambridge, 2001).
27. Gradstein, F., Ogg, J. & Smith, A. *A Geologic Timescale 2004* (Cambridge Univ. Press, Cambridge, 2004).
28. Oostendorp, C. *The Bryophytes of the Palaeozoic and Mesozoic* (J. Cramer, Berlin, 1987).
29. Veizer, J. *et al.* $^{87}Sr/^{86}Sr$, $\delta^{13}C$ and $\delta^{18}O$ evolution of Phanerozoic seawater. *Chem. Geol.* **161**, 59–88 (1999).
30. Katz, M. E. *et al.* Biological overprint of the geological carbon cycle. *Mar. Geol.* **217**, 323–338 (2005).

Acknowledgements

We thank H. Elderfield, D. Royer, P. Wilson and I. Woodward for helpful comments, M. Katz for the $\delta^{13}C_{carb}$ data sets, A. Ridgwell for the pH-corrected $\delta^{18}O$ data sets and H. Walker for stable-carbon-isotope analyses. We also thank the following for kindly providing fossil materials for isotopic analysis: A. Herman and V. Krassilov (Russian Academy of Sciences, Moscow), S. Wing and J. Wingerath (Smithsonian Institution, Washington), I. Daniel (University of Canterbury, Christchurch, New Zealand), A. Crame (British Antarctic Survey, Cambridge), P. Kenrick (Natural History Museum, London), W. G. Chaloner (University of London), D. Royer (Wesleyan University), J. McElwain (Trinity College, University of Dublin) and J. Francis (University of Leeds), who also provided Fig. 1d. We gratefully acknowledge financial support of this research through a University of Sheffield studentship to B.J.F., a University of Sheffield Divisional Directors award and a Leverhulme Trust award to D.J.B., and a DOE grant to R.A.B.
Correspondence and requests for materials should be addressed to D.J.B.
Supplementary Information accompanies this paper on www.nature.com/naturegeoscience.

Author contributions

B.J.F. conducted the geochemical and data analyses and drafted the manuscript, S.J.B. conducted data analyses, C.W.A. conceived and designed the uncertainty analyses and time-series comparisons, R.A.B. undertook the geochemical carbon-cycle modelling and D.J.B. planned the project, drafted the manuscript and undertook data analyses.